Climate Processes in CMIP5: Reasons for the Large Differences in Simulated Low-Level Jet among the CMIP5 Models

Qi Hu
School of Natural Resources, and Department of Earth and Atmospheric Sciences,
University of Nebraska-Lincoln, and
Song Feng
Department of Geosciences
University of Arkansas

(This research has been supported by NOAA Grant NA09OAR4310188 and
NSF Grant AGS-1103316 to the University of Nebraska-Lincoln)

The summertime southerly low-level jet (LLJ) from the Gulf of Mexico to the U.S. Great Plains and the Midwest refers to two different things. One is the climatology of the low-level (from the surface to ~700hPa) winds in that region, and the other is individual events of strong southerly winds in the region, which are sometimes, or often, associated with precipitation.

While the individual events contribute to the climatology of the LLJ, the prevailing southerly low-level winds in the region, with speed weaker than in the LLJ events, determine the LLJ climatology.

In this analysis, we focus on the climatology simulated by the CMIP5 models (not individual events).

Admittedly, there could be many factors affecting simulations of the LLJ climatology by individual GCMs. We focus on model simulated large-scale pressure in the lower troposphere in North America. The differences between the models that can and models that cannot simulate the LLJ well can help guide us to potential way(s) to improve the models in describing the LLJ.

Table 1: A list of the models used in this study with model resolution and origin.

Model	Resolution (degrees of long. by lat.)	Origin
BCC-CSM1.1	2.815×2.815	Beijing Climate Center, China
CanESM2	2.815×2.815	Canadian Centre for Climate, Canada
CCSM4	1.25×0.9	National Center for Atmospheric Research, USA
CNRM-CM5	1.40×1.40	Centre National de Recherches Meteorologiques, France
CSIRO-Mk3.6	1.875×1.875	Commonwealth Scientific and Industrial Research, Australia
GFDL-CM3	2.5×2.0	Geophysical Fluid Dynamics Laboratory, NOAA, USA
GFDL-ESM2M	2.5×2.0	Geophysical Fluid Dynamics Laboratory, NOAA, USA
GISS-E2-R	2.5×2.0	Goddard Institute for Space Studies, NASA, USA
HadGEM2-ES	1.875×1.25	Met Office Hadley Centre, UK
INM-CM4	2.0×1.5	Institute for Numerical Mathematics, Russia
IPSL-CM5A-LR	3.75×1.875	Institute Pierre-Simon Laplace, France
MIROC5	1.40×1.40	Atmosphere and Ocean Research Institute, Japan
MIROC-ESM	2.815×2.815	Japan Agency for Marine-Earth Science and Technology
MPI-ESM-LR	1.875×1.875	Max Planck Institute for Meteorology, Germany
MRI-CGCM3	1.125×1.125	Meteorological Research Institute, Japan
NorESM1-M	2.5×1.875	Norwegian Climate Centre, Norway

Table 2: Vertical levels in the NCEP/NCAR reanalysis data and in the five CMIP5 models.

Reanalysis/Models	Number of vertical levels	Pressure at the vertical levels (hPa)
NCEP-NCAR Reanalysis data	17 levels	1000, 925, 850, 700, 600, 500, 400, 300, 250, 200, 150, 100, 70, 50, 30, 20, 10
CCSM4	17 levels	1000, 925, 850, 700, 600, 500, 400, 300, 250, 200, 150, 100, 70, 50, 30, 20, 10
GFDL-CM3	23 levels	1000, 925, 850, 775, 700, 600, 500, 400, 300, 250, 200, 150, 100, 70, 50, 30, 20, 10, 7, 5, 3, 2, 1
GISS-ER	17 levels	1000, 925, 850, 700, 600, 500, 400, 300, 250, 200, 150, 100, 70, 50, 30, 20, 10
HadGEM2-ES	23 levels	1000, 925, 850, 700, 600, 500, 400, 300, 250, 200, 150, 100, 70, 50, 30, 20, 10, 7, 5, 3, 2, 1, 0.4
MPI-ESM-LR	25 levels	1000, 925, 850, 700, 600, 500, 400, 300, 250, 200, 150, 100, 70, 50, 30, 20, 10, 7, 5, 3, 2, 1, 0.4, 0.2, 0.1

Averaged summer 925hPa wind during 1971-2000 for a) NCEP-NCAR reanalysis, b) CCSM4, c) GFDL-CM3, d) GISS-E2-R, e) HadGEM2-CC and f) MPI-ESM-LR. g) and h) are showing the NARR results for different periods. Shadings indicate the meridional wind is larger than 3.0 m/s.

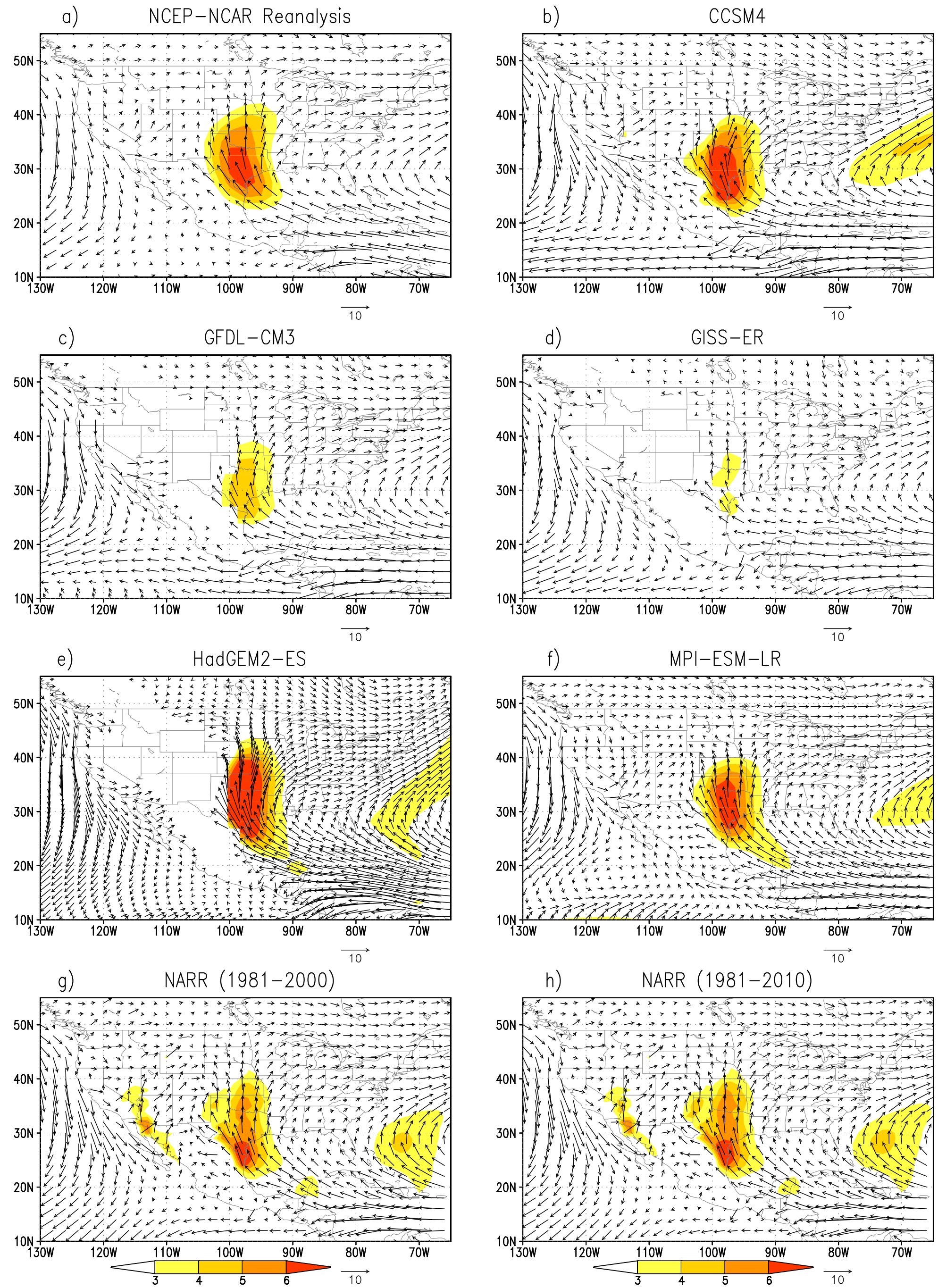

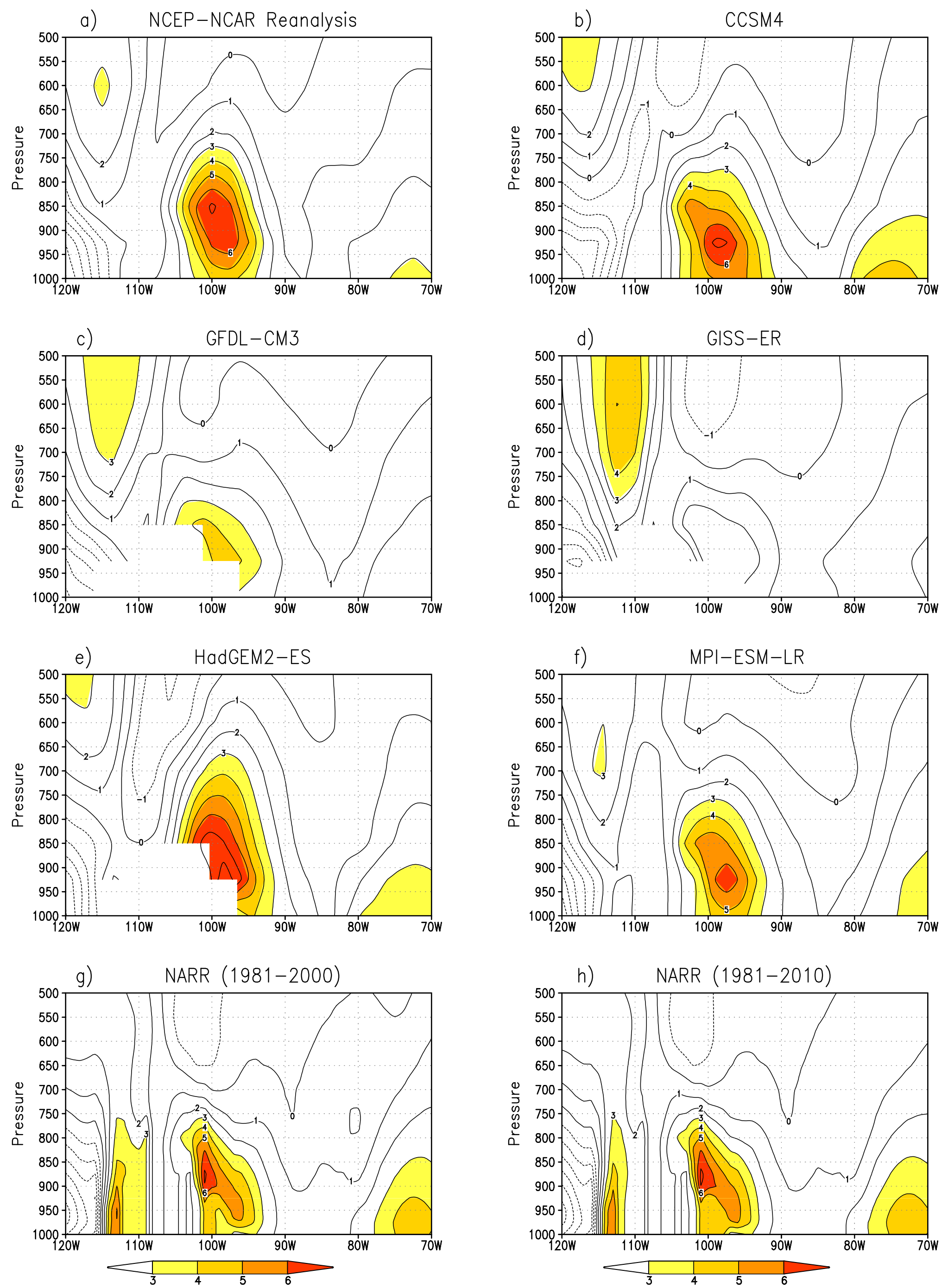

Cross-section of the summer meridional wind at 30N averaged during 1971-2000. Shadings indicate the meridional wind is larger than 3.0 m/s.

Seasonal variation of the long-term (1971-2000) mean meridional wind averaged over 95-100W. Shadings indicate meridional wind is larger than 3.0 m/s.

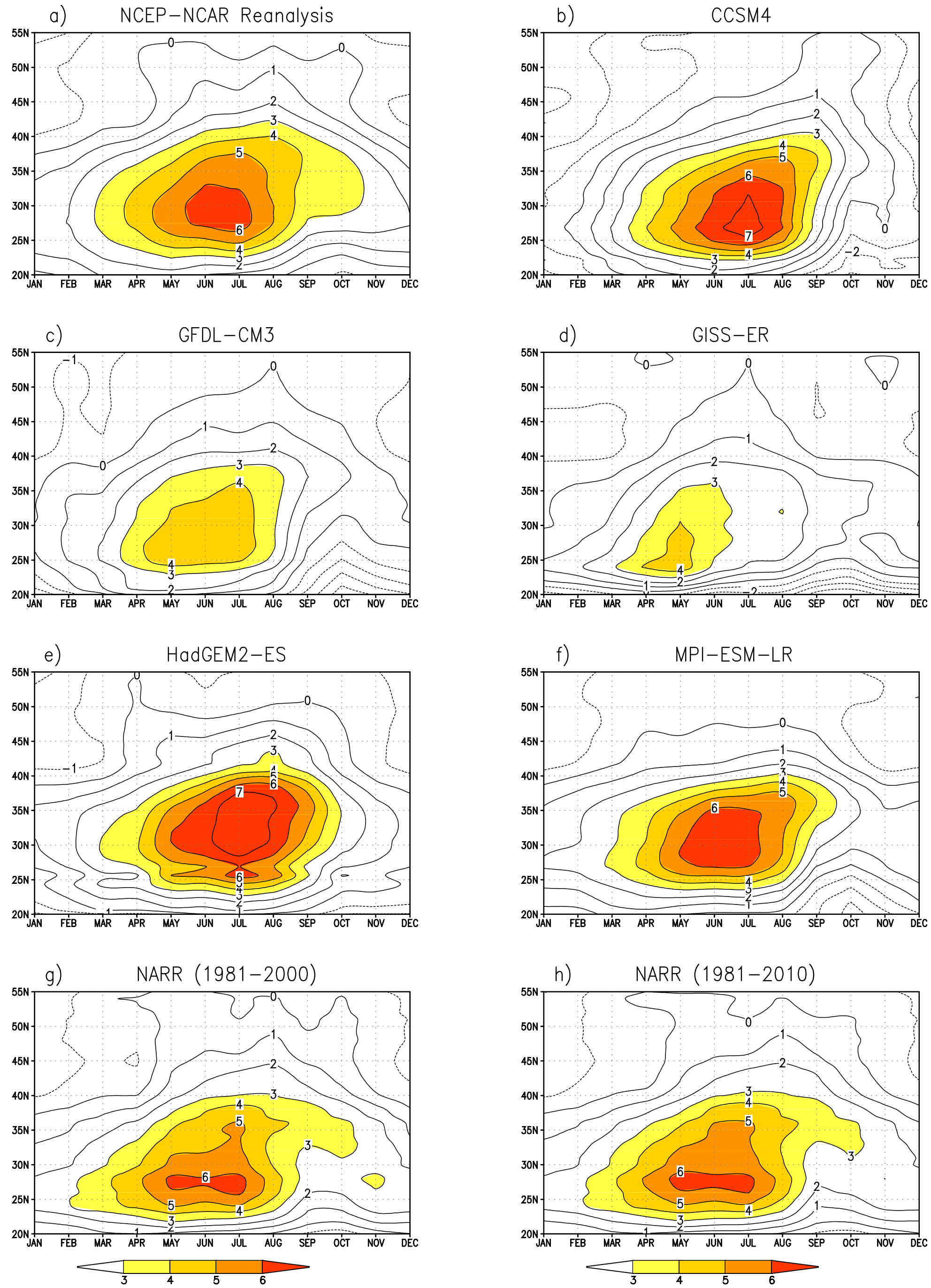

Table 3: Index of Agreement (D, D=1 is a perfect agreement) and RMSE from model comparisons with the reanalysis data. The comparisons were made for the areas confined by the square or rectangle in Figs. 5a, d, and g for spatial extent, vertical structure (intensity) and seasonal cycle, respectively. The "Average" is an average of the values of the three LLJ parameters.

Model	Index of Agreement (D)				RMSE			
	Vertical structure	Seasonal cycle	Spatial extent	Average	Vertical structure	Seasonal cycle	Spatial extent	Average
BCC-CSM1.1	0.886	0.939	0.909	0.911	1.387	1.128	1.113	1.209
CanESM2	0.947	0.962	0.940	0.950	0.874	0.854	0.872	0.867
CCSM4	0.947	0.962	0.941	0.950	0.907	0.884	0.862	0.884
CNRM-CM5	0.965	0.969	0.933	0.956	0.663	0.737	0.849	0.750
CSIRO-Mk3.6	0.930	0.978	0.948	0.952	0.995	0.618	0.751	0.788
GFDL-CM3	0.844	0.876	0.893	0.871	1.099	1.370	0.900	1.123
GFDL-ESM2M	0.925	0.933	0.923	0.927	0.902	1.013	0.849	0.921
GISS-ER	0.671	0.747	0.677	0.698	1.732	2.102	1.618	1.817
HadGEM2-ES	0.922	0.948	0.945	0.938	1.063	0.983	0.836	0.961
INM-CM4	0.829	0.913	0.849	0.864	1.624	1.209	1.233	1.355
IPSL-CM5A-LR	0.853	0.823	0.814	0.830	1.239	1.733	1.393	1.455
MIROC5	0.913	0.975	0.932	0.940	1.121	0.652	0.879	0.884
MIROC-ESM	0.827	0.855	0.808	0.830	1.701	1.864	1.703	1.756
MPI-ESM-LR	0.949	0.959	0.939	0.949	0.757	0.851	0.773	0.794
MRI-CGCM3	0.898	0.890	0.902	0.897	1.038	1.283	0.920	1.080
NorESM1-M	0.908	0.939	0.918	0.922	1.263	1.137	1.041	1.147

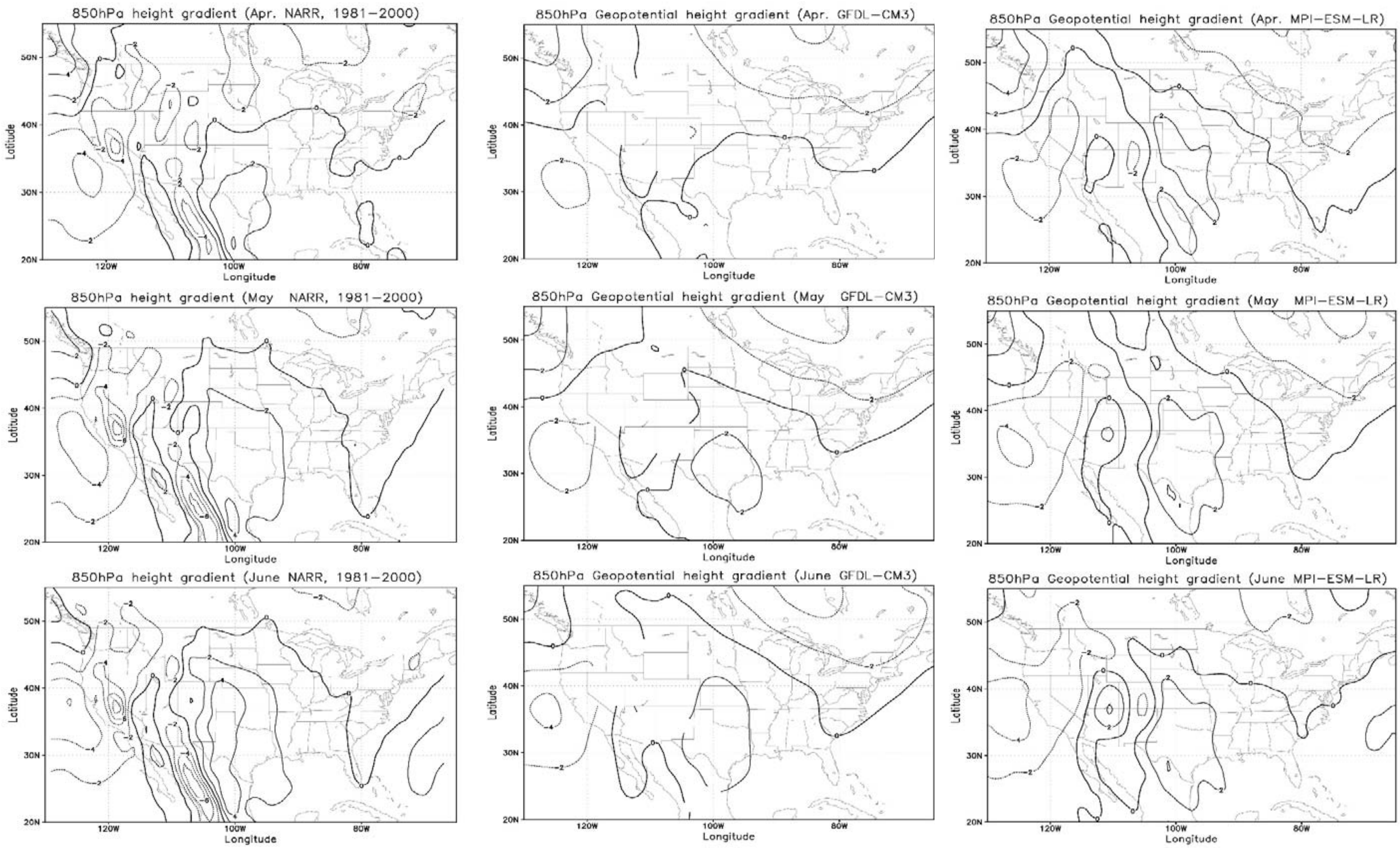

850hPa height gradient (Apr. NARR, 1981−2000)
850hPa Geopotential height gradient (Apr. GFDL−CM3)
850hPa Geopotential height gradient (Apr. MPI−ESM−LR)
850hPa height gradient (May NARR, 1981−2000)
850hPa Geopotential height gradient (May GFDL−CM3)
850hPa Geopotential height gradient (May MPI−ESM−LR)
850hPa height gradient (June NARR, 1981−2000)
850hPa Geopotential height gradient (June GFDL−CM3)
850hPa Geopotential height gradient (June MPI−ESM−LR)
Latitude
Longitude
20N
30N
40N
50N
120W
100W
80W

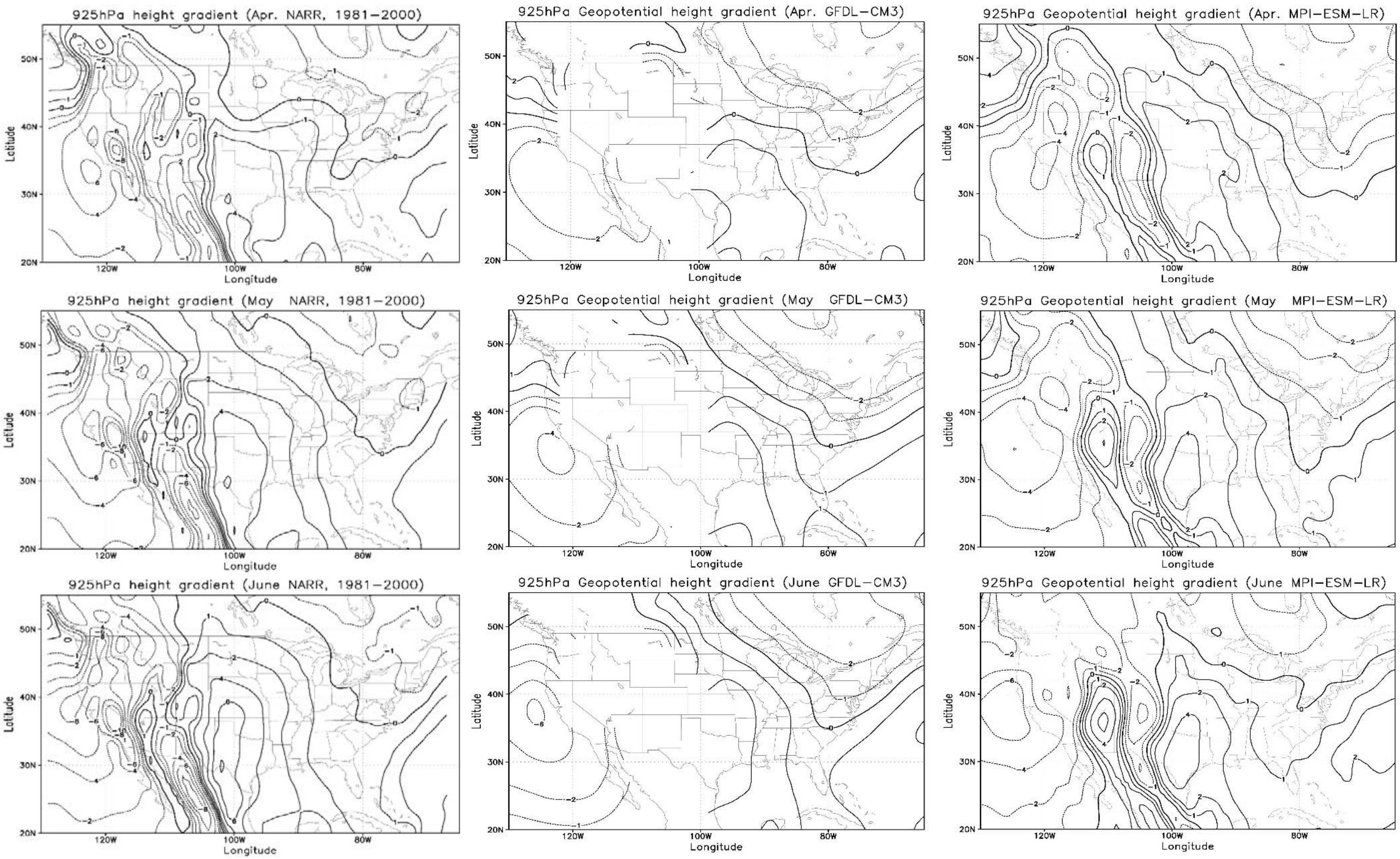
925hPa height gradient (Apr. NARR, 1981-2000)
925hPa Geopotential height gradient (Apr. GFDL-CM3)
925hPa Geopotential height gradient (Apr. MPI-ESM-LR)
925hPa height gradient (May NARR, 1981-2000)
925hPa Geopotential height gradient (May GFDL-CM3)
925hPa Geopotential height gradient (May MPI-ESM-LR)
925hPa height gradient (June NARR, 1981-2000)
925hPa Geopotential height gradient (June GFDL-CM3)
925hPa Geopotential height gradient (June MPI-ESM-LR)
Latitude
Longitude
50N
40N
30N
20N
120W
100W
80W

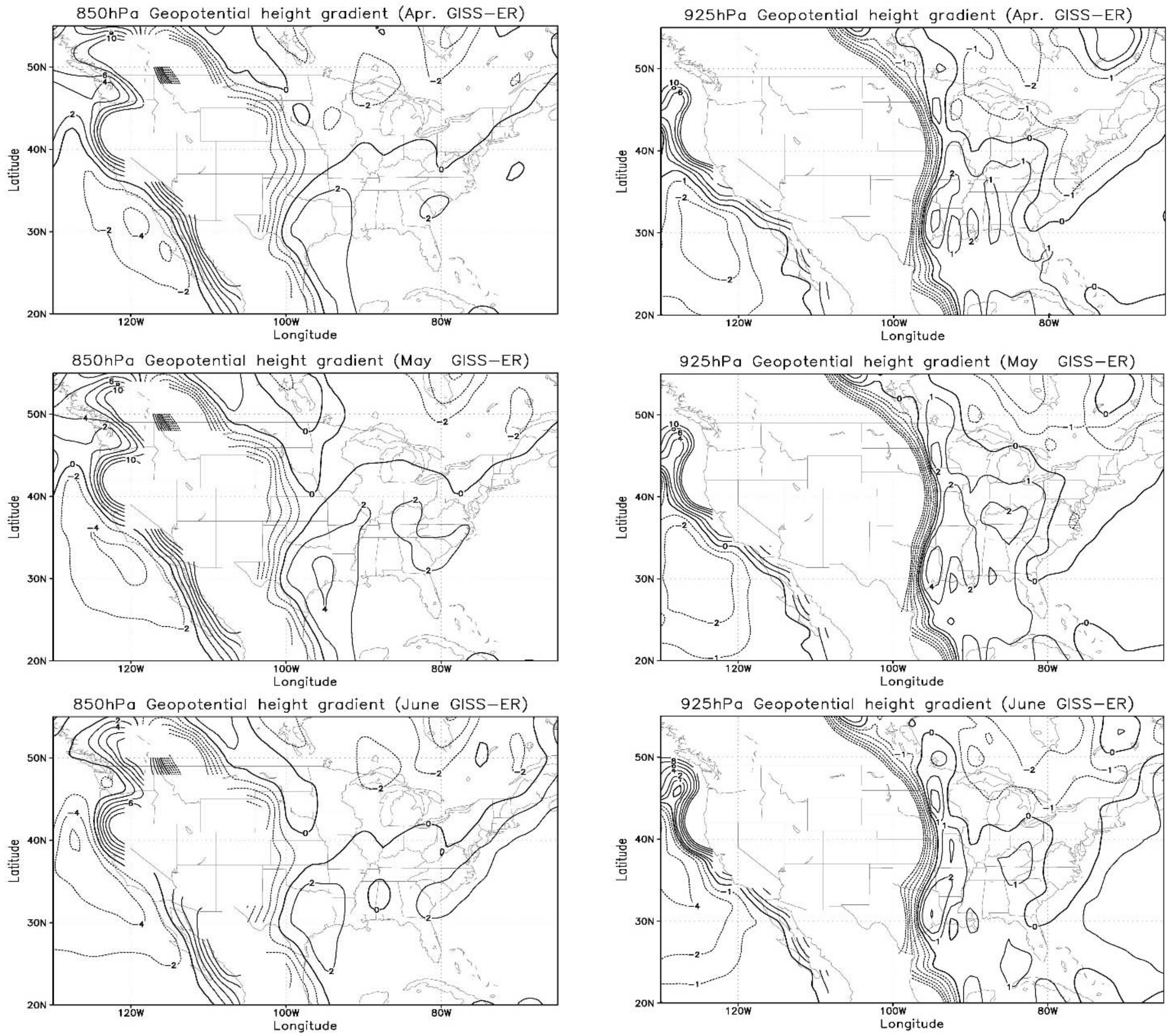
850hPa Geopotential height gradient (Apr. GISS-ER)
925hPa Geopotential height gradient (Apr. GISS-ER)
850hPa Geopotential height gradient (May GISS-ER)
925hPa Geopotential height gradient (May GISS-ER)
850hPa Geopotential height gradient (June GISS-ER)
925hPa Geopotential height gradient (June GISS-ER)
Latitude
Longitude
20N
30N
40N
50N
120W
100W
80W

Summary

The LLJ is a shallow system in the lower troposphere. For such system, it is most likely that the winds are adjusting to the pressure field. The pressure distribution/variation results primarily from the thermodynamic processes. Therefore, accurately describing those processes would be essential for models to improve simulations of the LLJ. The thermodynamic processes could include heating at the surface and partition of the heating into sensible and latent heat, the orographic effects on surface heating, and boundary layer exchange with the free atmosphere.

Some of these are the subjects of examination in this study.